

# Synthesis, characterization and application of zinc oxide nano particles for removal of hexavalent chromium

Mayank Pandey<sup>1,2</sup> · B. D. Tripathi<sup>3</sup>

Received: 19 April 2016 / Accepted: 9 June 2016 / Published online: 7 July 2016  
© Springer Science+Business Media Dordrecht 2016

**Abstract** The present study was conducted to evaluate the adsorption efficiency of synthesized nano zinc oxide (n-ZnO) for the removal of hexavalent chromium ( $\text{Cr}^{6+}$ ). The synthesized sample was characterized by X-ray diffraction, Fourier transform infrared spectroscopy, and scanning electron microscopy. Batch experiment results revealed that low dose ( $4 \text{ g L}^{-1}$ ) of n-ZnO was highly efficient at the initial metal concentration of  $9 \text{ mg L}^{-1}$  in acidic conditions (pH 2) at  $50 \text{ }^\circ\text{C}$  for the contact time of 90 min. A Langmuir adsorption isotherm model was found to be best fitted indicating a homogeneous surface and the adsorption followed pseudo-second order kinetics. Intra-particle diffusion was not a rate limiting factor in the present study. Thermodynamic study revealed that the adsorption process was endothermic and spontaneous at all the studied temperatures with increasing randomness.

**Keywords** Characterization · Chromium · Nano zinc oxide (n-ZnO) · Removal efficiency · Adsorption

---

✉ B. D. Tripathi  
tripathibd@gmail.com

Mayank Pandey  
mayankacademics@gmail.com

<sup>1</sup> Institute of Environment and Sustainable Development, Banaras Hindu University, Varanasi 221005, India

<sup>2</sup> Present Address: Department of Environmental Studies, P.G.D.A.V. College (Evening), University of Delhi, New Delhi 110065, India

<sup>3</sup> Department of Botany for Advanced Studies, Banaras Hindu University, Varanasi 221005, India

## Introduction

With fast urbanization and rapid industrialization, the amount of wastewater discharged has become a serious environmental threat and challenging task. The presence of various forms of metals in wastewater beyond the permissible limit adversely affects the environment and public health eventually leading to an ecological imbalance [1]. It is well established that unlike organic pollutants, very slow natural degradation rates and the long half-life periods of metals are the real causes behind the accumulation and toxicity of metals [2]. Undergoing various cycles, metals enter the food chain/web and ultimately cause adverse physical and physiological effects on biotic elements of earth [3, 4]. Therefore, it is the time to synthesize highly efficient, cost effective, and environmentally friendly materials, which can be used for metal remediation at pilot and large scales.

Chromium (Cr) occurs in nature in the form of a stable oxide chromite trivalent [5]. Cr (Greek *Chroma*; means color) has wide applicability in different industrial sectors like chrome plating, textile and dyeing industries, tanneries, wood and furniture, etc. [6]. Cr occurs in two principal oxidation states, i.e., trivalent (+3), which is biologically essential and hexavalent forms (+6), which are mutagenic in nature. In aqueous medium, Cr<sup>3+</sup> exists in neutral [Cr<sub>3</sub>(OH)<sub>4</sub>]<sup>0</sup>, mononuclear [Cr(OH)<sup>2+</sup>, Cr(OH)<sub>2</sub><sup>+</sup>, Cr(OH)<sub>3</sub>] and polynuclear forms [Cr<sub>2</sub>(OH)<sub>2</sub>], while Cr<sup>6+</sup> remains predominantly in anionic forms (CrO<sub>4</sub><sup>2-</sup>, HCrO<sub>4</sub><sup>2-</sup>, Cr<sub>2</sub>O<sub>7</sub><sup>2-</sup>). Cr<sup>6+</sup> is toxic and has higher solubility and mobility than Cr<sup>3+</sup> in aqueous media. USEPA has prescribed 100 µg L<sup>-1</sup> Cr<sup>6+</sup> in drinking water; consumption in higher doses may lead to skin problems, diarrhea, gastric problems, liver and kidney damage, internal hemorrhages, etc. [7, 8]. In acidic conditions, Cr<sup>6+</sup> exists in Cr<sub>2</sub>O<sub>7</sub><sup>2-</sup> while in an alkaline environment, the CrO<sub>4</sub><sup>2-</sup> form is predominant [9]. In India, the maximum permissible limit for Cr<sup>6+</sup> in drinking water is 0.05 mg L<sup>-1</sup>. The Bureau of Indian Standards (BIS) has also given standards for the discharge of Cr<sup>6+</sup> in inland surface water (0.1 mg L<sup>-1</sup>), public sewage (2 mg L<sup>-1</sup>), and marine/coastal areas (1 mg L<sup>-1</sup>) [10].

Different methodologies like reverse osmosis, ion exchange, and adsorption have been adopted for the remediation of hexavalent Cr from aqueous solutions [11]. Workers around the world have applied various materials as low cost adsorbents for Cr remediation, viz., almond, groundnut, walnut, and coconut shell [9, 12–16, 65], rice husk, and straw [17–19], palm flower and oil palm waste [20, 21], river bed sand [22, 23], activated spent clay [24], Wollastonite [25], algal sp. [26–28], etc. Although low cost adsorbents have been proved as potent candidates for water purification, many synthesized nano sized metal oxides have emerged as efficient adsorbents. Nano sized metal oxides are better adsorbents because of large surface area and high activity due to the size quantization effect [14, 29–33]. Various metal oxides used in wastewater/water treatment are hydrous and anhydrous iron oxides (Fe<sub>3</sub>O<sub>4</sub>, Fe<sub>2</sub>O<sub>3</sub>) [34–39], hydrous and anhydrous manganese oxides [36, 40–42], and titanium oxide (TiO<sub>2</sub>) [43].

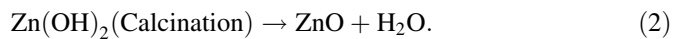
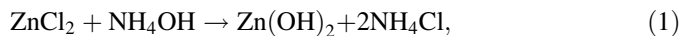
The efficiency of nano sized zinc oxide (n-ZnO) is yet to be explored, as little work has been done on its synthesis and application for water purification [44–46].

Nano ZnO (n-ZnO) are believed to be environmentally friendly and can be applied in various fields such as the catalyst industry [47], solar cells [48] and gas sensors [49], etc. Earlier, it was used for H<sub>2</sub>S removal, but later it was recognized as a potent metal adsorbent [32, 50]. Therefore, synthesis and application of ZnO for Cr<sup>6+</sup> removal from wastewater was considered in the present study. The present study was conducted at the Pollution Ecology Research Laboratory, Department of Botany, Banaras Hindu University, Varanasi (India).

## Materials and methods

### Synthesis of zinc oxide nano particles

The nano sized zinc oxide (n-ZnO) synthesis scheme was broadly based upon the experimental design as discussed elsewhere [51]. All the reagents procured were of analytical grade. A 10 ml solution of 0.08 M Cetriammonium bromide (CTAB-cationic surfactant) was added to 500 ml 0.5 M zinc chloride solution (ZnCl<sub>2</sub>). Liquid ammonia solution (10 ml, NH<sub>4</sub>OH) was added slowly to the homogenous ZnCl<sub>2</sub>-CTAB solution with continuous stirring. After stirring (4 h), the solution was left for 4 days (96 h) to get an aged sample. After aging, the samples were filtered, washed with double distilled water (to remove surfactant), and dried at room temperature. Air dried samples were calcined in a tubular muffle furnace at 450 °C for 2 h. The above steps can chemically be represented as [44]



Ammonium chloride (NH<sub>4</sub>Cl) and hydroxide ions (OH<sup>-</sup>) evaporated in the form of ammonia gas and water vapours, respectively. The diagrammatic scheme illustration is given in Fig. 3c.

### Batch studies

Batch studies were conducted to assess the removal efficiency (RE) of n-ZnO. The effect of pH, initial metal concentration, temperature, time, and dose was investigated. Cr<sup>6+</sup> solutions of desired concentrations were prepared from a 1000 mg L<sup>-1</sup> Cr<sup>6+</sup> stock solution. The pH of solutions was adjusted using dilute acid (HCl) and alkaline solutions (NaOH). The adsorption capacity and efficiency of n-ZnO was calculated using Eqs. 3 and 4, respectively.

$$q_e = [(C_i - C_e)](V/W), \quad (3)$$

$$\text{Removal efficiency percentage (RE \%)} = [(C_i - C_e)/C_i] \times 100, \quad (4)$$

where  $q_e$  is the amount of adsorbate ( $\text{Cr}^{6+}$ ) on per unit mass of adsorbent (n-ZnO) ( $\text{mg g}^{-1}$ ),  $C_i$  and  $C_e$  are initial and equilibrium concentrations of adsorbate ( $\text{mg L}^{-1}$ ),  $V$  is volume of metal solution (ml), and  $W$  is mass of adsorbent (mg).

## Results and discussion

### Characterization of n-ZnO

X-ray diffraction analysis (XRD) [RIGAKU-Miniflex II diffractometer adopted  $\text{Cu-K}\alpha$  radiation ( $\lambda = 1.5405 \text{ \AA}$ ) with a tube voltage of 40 kV and current of 35 mA in a  $2\theta$  range between  $20^\circ$  and  $80^\circ$ ] was conducted. The step size and measuring speed was set to  $0.02^\circ$  and  $1^\circ$  per min, respectively, in the present investigation. The JCPDS-International Centre for Diffraction Data Cards were used as a reference. Prominent diffraction peaks (Fig. 1) were found at  $31.74$  (100),  $34.36$  (002),  $36.16$  (101),  $47.48$  (102),  $56.74$  (110),  $62.81$  (103),  $67.93$  (112), and  $69.17$  (201), which matched with JCPDS card 36-1451. This confirmed that the synthesized material was ZnO formed by the co-precipitation method. The average crystalline size range was obtained by the Sherrer equation, which can be mathematically expressed as:

$$D = (k\lambda)/(\beta \cos \theta), \quad (5)$$

where  $D$  is the average crystalline size (nm),  $k$  is a constant (0.89),  $\lambda$  is the wavelength ( $1.54 \text{ \AA}$ ),  $\beta$  is full width at half maxima (FWHM), and  $\theta$  is the Bragg diffraction angle. The average crystalline size range was found to be between 26.28 and 56.77 nm.

The presence of functional groups also alters the removal efficiency of the adsorbent. A Fourier transform infrared spectroscopy (FTIR) (Perkin Elmer

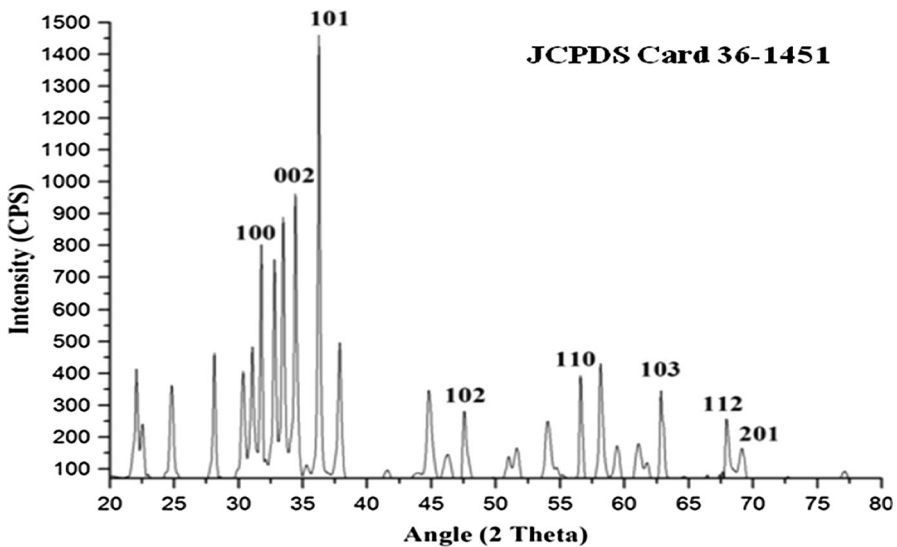


**Fig. 1** X-ray diffraction of n-ZnO

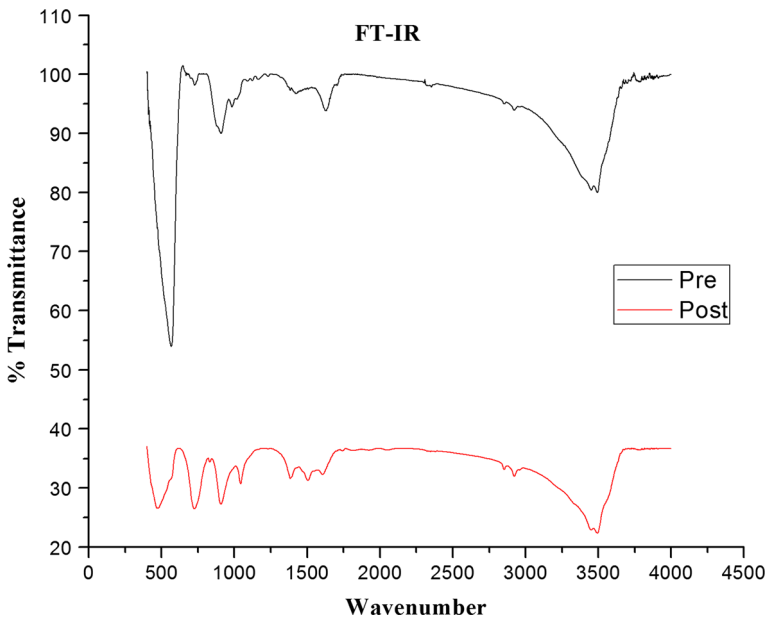


**Fig. 2** FT-IR spectrum of pre- and post-treated n-ZnO

spectrum version 10.03.05) study was conducted on the adsorbent, before and after the treatment, to identify the presence and detect the change in the functional groups (Fig. 2). Wave number  $2800\text{--}3000\text{ cm}^{-1}$  represents C–H absorption and  $3500\text{ cm}^{-1}$  represents OH bonds while  $567\text{ cm}^{-1}$  peak reflects ZnO.

The surface area of the adsorbent is an important parameter to assess its efficiency. The surface area of synthesized n-ZnO was assessed using a surface area analyzer. The surface area was found to be  $18.39\text{ m}^2\text{g}^{-1}$ , which showed a good agreement with the findings of Wang et al. [51] ( $17.6\text{ m}^2\text{g}^{-1}$ ). The surface morphology of ZnO depends upon various external factors like synthesis technique and process, pH, and precursors, etc. Therefore, surface morphology change studies are a must to assess the efficiency of metal oxide adsorbents [52]. The change in surface morphology of the adsorbent (n-ZnO) was investigated using a scanning electron microscope (SEM) (FEI Quanta 200F) (Fig. 3a, b). Although the principal fraction of particles formed was almost spherical in shape, some needle- and rod-shaped particles were also observed. A rough surface of unused n-ZnO particles depicts the presence of numerous active sites, which are occupied by metal ions ( $\text{Cr}^{6+}$ ) after adsorption making the adsorbent surface smooth.

## Batch study

### *Effect of pH*

The pH plays a vital role in deciding the morphology and efficiency of adsorbents. In the present study, the RE of the adsorbent was assessed at different pH (2, 4, 6, 8,

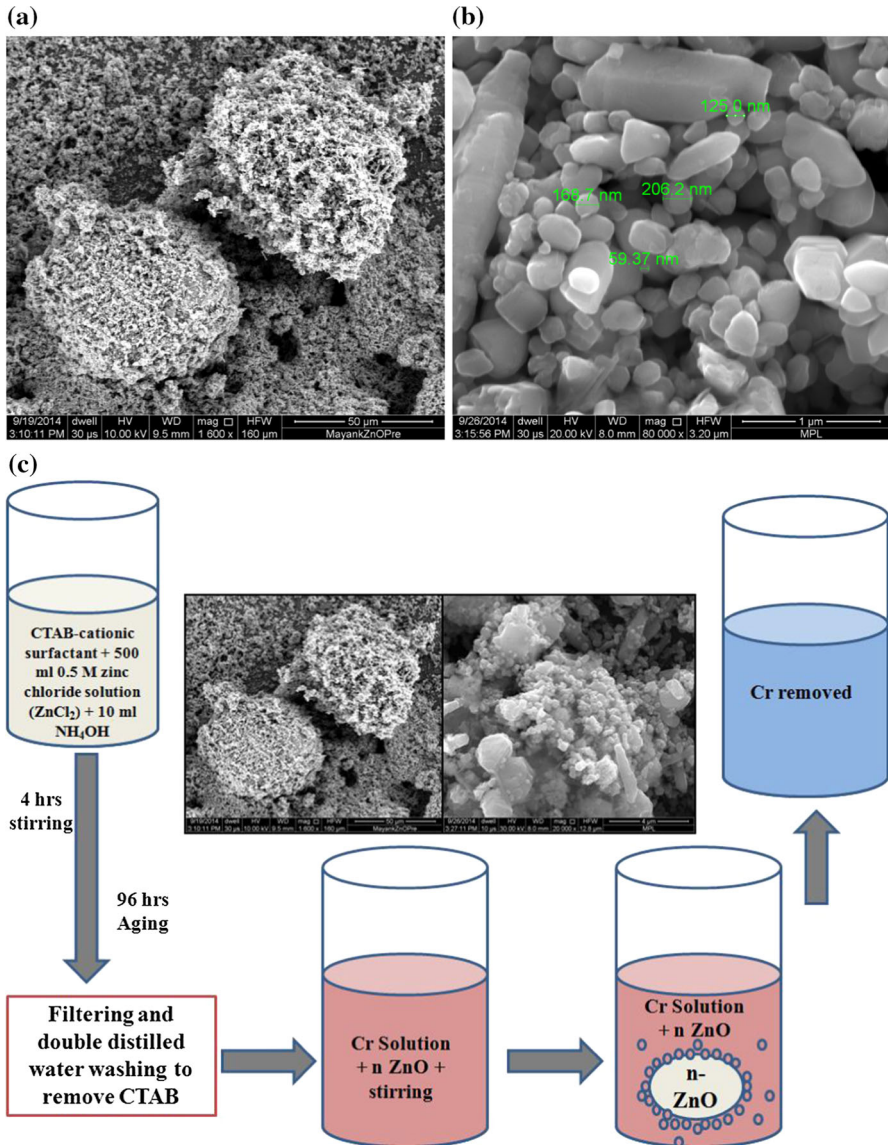


**Fig. 3** SEM micrograph of **a** untreated and **b** treated n-ZnO. **c** Scheme illustration of  $\text{Cr}^{6+}$  adsorption

and 10). Study revealed that at pH 2.0, the maximum removal efficiency was 100 %, which steeply decreases with the increase in pH and around 55 % Cr is adsorbed at highly alkaline pH (10.0) (Fig. 4). It is well documented that at acidic conditions, the adsorbent surface becomes positively charged (protonation), which chemically attracts the  $\text{Cr}^{6+}$  present in various anionic forms ( $\text{CrO}_4^{2-}$ ,  $\text{Cr}_2\text{O}_7^{2-}$ ). In alkaline conditions deprotonation occurs, which adversely affects  $\text{Cr}^{6+}$  adsorption. The

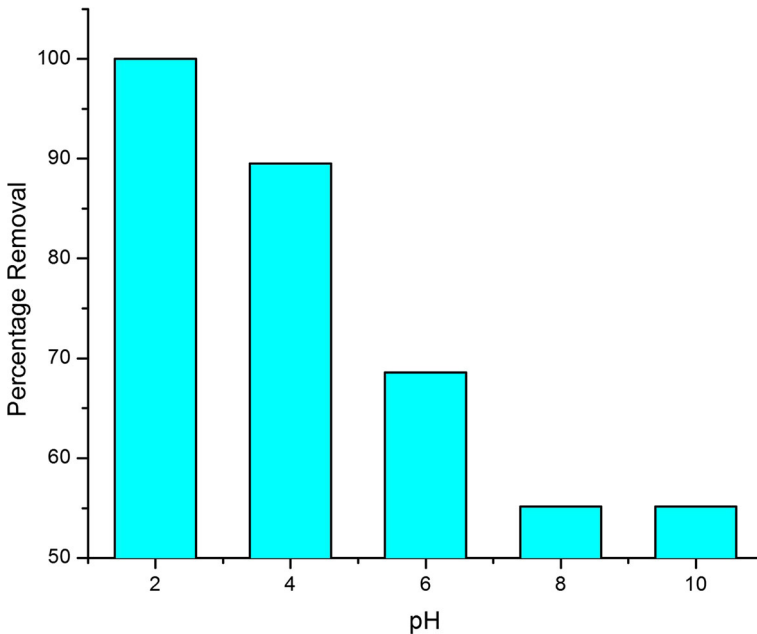


**Fig. 4** Effect of pH

chemical equilibrium equation showing the relationship between different Cr anions [9]:



Adsorption in neutral and alkaline conditions may be due to reasons other than electrostatic interaction. Similar results have been reported by different workers using different adsorbents [9, 23, 53].

Illumination increases the dissolution rate of ZnO but is a slow process [54]. Direct contact of UV–visible light with n-ZnO was prevented to avoid photocorrosion and decomposition of the adsorbent. However, Zhang [55] mentioned that under highly acidic and alkaline conditions, the corrosion film formed on Zn is very loose. Since the contact period in the present study is too small, the dissolution, solubility, and corrosion of ZnO would have been negligible to cause adverse effects on its removal efficiency.

It has been very well established that dissolution of n-ZnO at low and high pH is a size dependent phenomenon and also affected by the adsorbing species [54, 69, 70]. Since we have performed the batch experiment at particle sizes ranging from ~50 to ~300 nm and observed maximum removal at low pH value and negligible leaching of Zn ion from ZnO at this pH (figure not shown); therefore, it can be concluded that adsorbent was stable at this pH. This is more likely to result due to very high affinity of  $\text{Cr}^{6+}$  for n-ZnO or rapid attack of  $\text{Cr}^{6+}$  on active sites present on the nano-adsorbent surface.

*Effect of initial metal concentration, contact time, and dose of adsorbent*

$\text{Cr}^{6+}$  removal efficiency percentage of n-ZnO as the function of initial metal concentration was investigated on standard solutions of various concentrations (1–10, 15, 20, 30, 40, and 50  $\text{mg L}^{-1}$ ). The n-ZnO showed 100 % removal efficiency at a metal concentration of 9  $\text{mg L}^{-1}$  and decreases gradually on further increasing the metal concentration. The least RE % (79.53 %) was obtained at 50  $\text{mg L}^{-1}$  depicting the low adsorption capacity of adsorbent at higher concentration. The necessary driving force to overcome the mass transfer resistance for adsorbate between the solution and solid phases is provided by the initial metal ion concentration [56]. As the initial metal ion concentration at the same adsorbent dose increases, the availability of active sites decreases, which, consequently, decreases the removal efficiency percentage (Fig. 5).

Contact time imparts a significant effect on removal efficiency of adsorbents. Effect of contact time was assessed by running the experiment for different time periods (5, 10, 15, 20, 25, 30, 45, 60, 90, 120, and 180 min) at different metal ion concentrations (10, 20, and 30  $\text{mg L}^{-1}$ ). Increase in RE % was observed (Fig. 6) with increase in contact time from 5 min (7.8, 17.68, and 20.4 %) to 90 min (100, 90.94, and 89.02 %) and remained constant thereafter at different adsorbate concentrations (10, 20, and 30  $\text{mg L}^{-1}$ ). Therefore, 90 min contact time was selected as equilibrium for maximum removal.

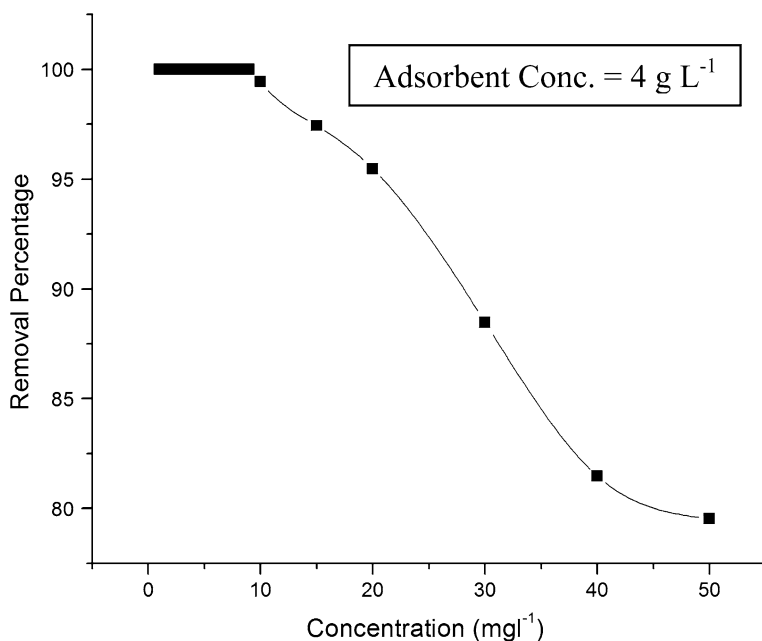


**Fig. 5** Effect of initial metal ion concentration



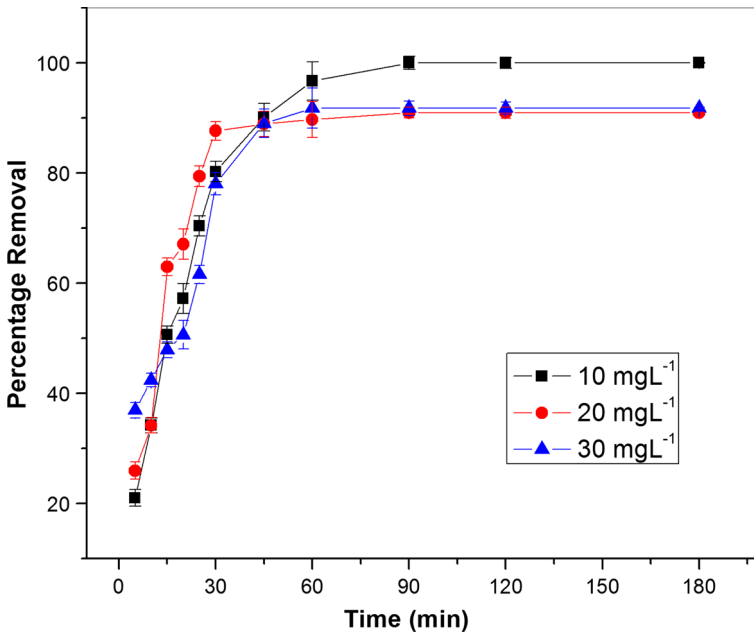


**Fig. 6** Effect of time

RE % increases with the increase in adsorbent dose and reached up to maximum at  $4 \text{ g L}^{-1}$ , after which it remained nearly constant (Fig. 7). Increase in RE % with increase in adsorbent dose may be due to an increment in the number of active sites for adsorption.

#### *Effect of temperature*

Effect of temperature on adsorption efficiency was assessed by executing the batch experiments at various temperatures (30, 40, and 50 °C) at different metal ion concentration (10, 20, 30, 40, 50, and 60  $\text{mg L}^{-1}$ ) (Fig. 8). Maximum RE was obtained at the highest temperature (50 °C) for all the concentrations. This depicts the endothermic nature of the adsorbent [53].

#### **Adsorption isotherm modelling**

The isotherm model reveals the relationship between concentration of metal ions adsorbed onto the surface of adsorbent and concentration of metal ions in liquid phase. To assess the adsorption capacity, two isotherm models, viz., Langmuir and Freundlich were applied to the present study data set having application concentration ranges viz. 0.5, 1, 1.5, 2, 2.5, 5, 10, 20, and 50  $\text{mg L}^{-1}$ .

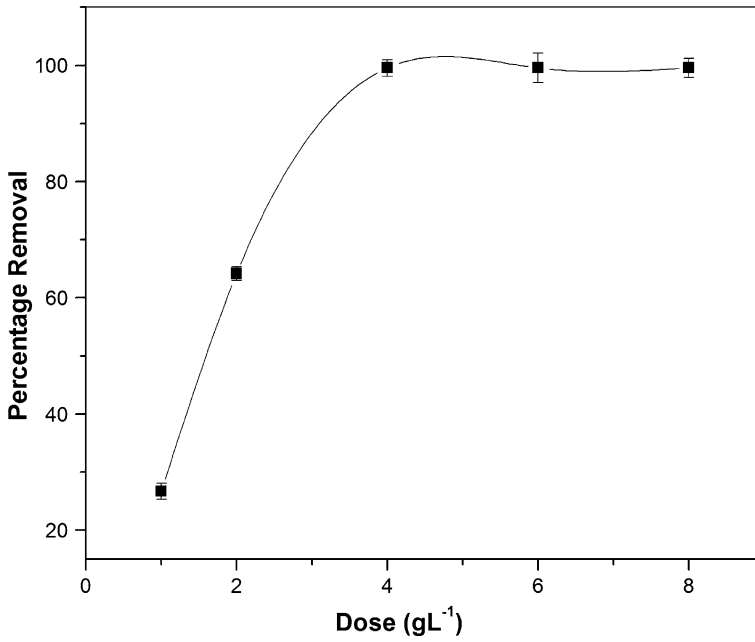


Fig. 7 Effect of dose

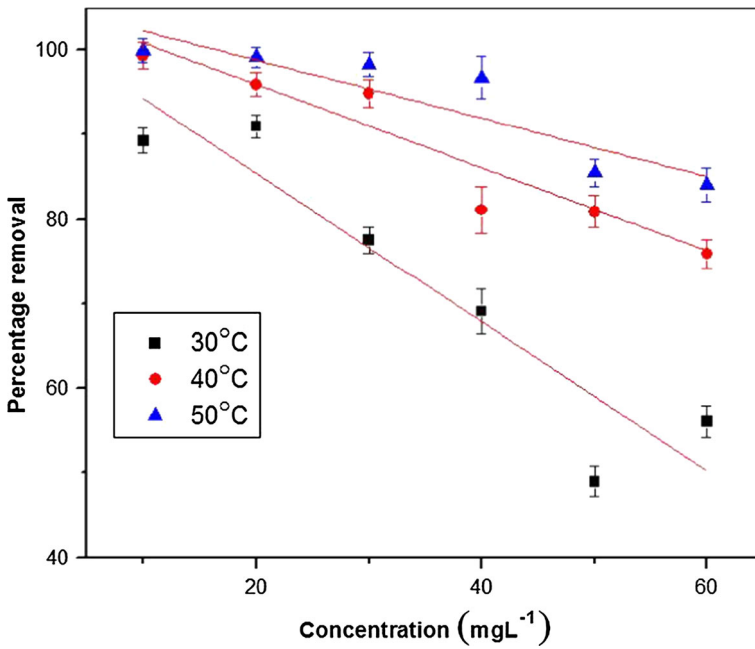
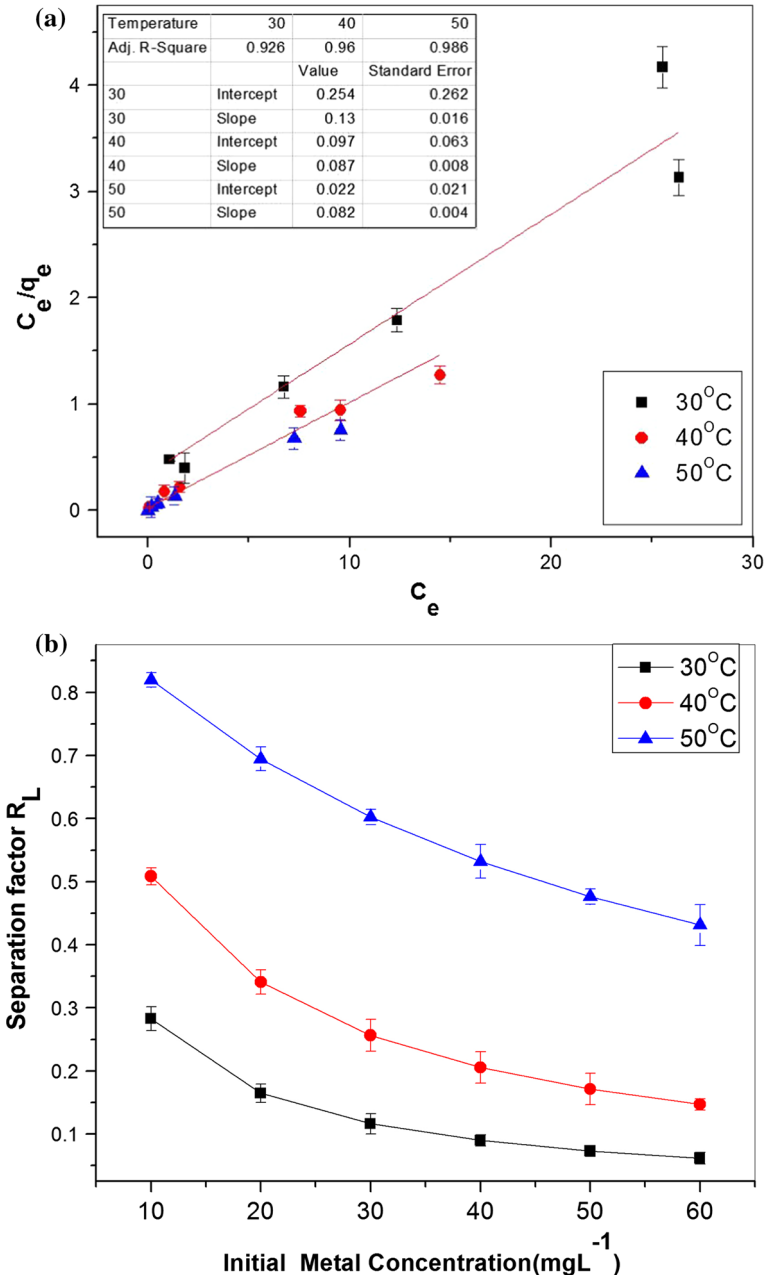


Fig. 8 Effect of temperature



**Fig. 9** a Langmuir isotherm model. b Separation factor at different temperatures. c Freundlich isotherm model

*Langmuir isotherm model*

The Langmuir isotherm model for single metal adsorption was given by Langmuir (1916), the non-linear form of which can be mathematically expressed as Eq. (6) [57]. To obtain maximum adsorption capacity ( $q_{max}$ ) and adsorption efficiency ( $b$ ), the linear form of Eq. (6) is required, which can be written as Eq. (7) [16]:

$$q = q_{max}[(bc_e)/(1 + bc_e)], \tag{6}$$

$$(c_e/q_e) = [1/(q_{max}b)] + (c_e/q_{max}), \tag{7}$$

where  $q_{max}$  is the maximum metal concentration adsorbed by per unit mass of adsorbent ( $mg\ g^{-1}$ ) having a homogenous surface at the equilibrium concentration of metals ( $c_e$ ) ( $mg\ L^{-1}$ ), when the surface of the adsorbent is full with metals ( $q_{max}$ ) ( $mg\ g^{-1}$ ) and  $b$  ( $L\ mg^{-1}$ ) is adsorption efficiency (affinity of adsorption). When the linear graph is plotted between  $c_e$  and  $c_e/q_e$ , the obtained  $q_{max}$  and  $b$  are calculated using the slope and intercept of the graph. The reciprocal of slope ( $1/slope$ ) gives  $q_{max}$  and the reciprocal of product of intercept and  $q_{max}$  gives  $b$ . In the present study, the maximum adsorption capacity ( $q_{max}$ ) of the adsorbent was  $12.2\ mg\ g^{-1}$  at  $50\ ^\circ C$  with  $R^2$  value near to unity (0.986) (Fig. 9a; Table 1).

The feasibility of the Langmuir model can be assessed by a dimensionless separation factor or equilibrium parameter ( $R_L$ ), which can be mathematically expressed as Eq. (8) [56, 58]:

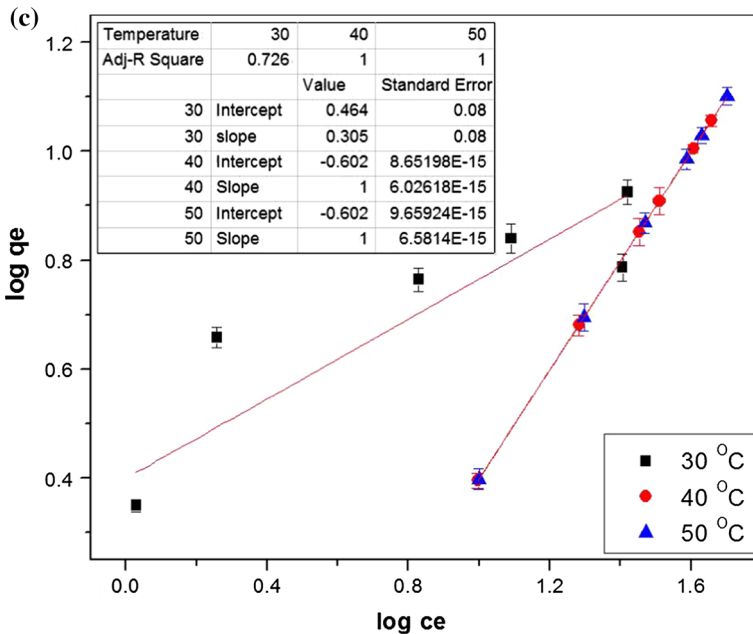


Fig. 9 continued

**Table 1** Adsorption isotherm and kinetic model parameters at different temperatures and concentrations

| Model               | Temperature (°C)                    | $q_{max}$ (mg g <sup>-1</sup> ) (1/slope)            | $b$ (L g <sup>-1</sup> ) (1/intercept × $q_{max}$ ) |   | $R^2$ |       |
|---------------------|-------------------------------------|--|---|---|-------|-------|
| Langmuir            | 30                                  | 7.7  | 0.511   |   | 0.926 |       |
|                     | 40                                  | 11.4   | 0.909   |   | 0.958 |       |
|                     | 50                                  | 12.2   | 3.75  |   | 0.986 |       |
| Freundlich          | Temperature (°C)                    | $k_f$ (mg g <sup>-1</sup> ) (Intercept = log $k_f$ ) | n (1/slope)   | $R^2$   |       |       |
|                     | 30                                  | 2.91   | 3.28  | 0.726   |       |       |
|                     | 40                                  | 0.25   | 1   | 1   |       |       |
|                     | 50                                  | 0.25   | 1   | 1   |       |       |
| Pseudo-first order  | Concentration (mg L <sup>-1</sup> ) | Experimental $q_e$ (mg g <sup>-1</sup> )             | Model $q_e$ (mg g <sup>-1</sup> )                   | $K_1$ (min <sup>-1</sup> )                    | $R^2$ |       |
|                     | 10                                  | 10   | 2.96  | $57.87 \times 10^{-3}$                        | 0.990 |       |
|                     | 20                                  | 18.19  | 6.64  | $89.21 \times 10^{-3}$                        | 0.873 |       |
|                     | 30                                  | 26.70  | 9.26  | $75.14 \times 10^{-3}$                        | 0.862 |       |
| Pseudo-second order | Concentration (mg L <sup>-1</sup> ) | Experimental $q_e$ (mg g <sup>-1</sup> )             | Model $q_e$ (mg g <sup>-1</sup> )                   | $K_2$ (g mg <sup>-1</sup> min <sup>-1</sup> ) | H     | $R^2$ |
|                     | 10                                  | 10   | 3.3   | 0.012   | 0.136 | 0.982 |
|                     | 20                                  | 18.19  | 13.86   | 0.004   | 0.91  | 0.775 |
|                     | 30                                  | 26.70  | 21.63   | 0.015   | 7.5   | 0.998 |

$$R_L = 1/(1 + b \times C_i). \tag{8}$$

The  $R_L$  value determines the shape of the isotherm, which varies from  $R_L > 1$  (unfavourable),  $R_L = 1$  (linear),  $0 < R_L < 1$  (favourable). In the present system,  $R_L$  values for the wide initial metal concentration range (10, 20, 30, 40, 50, and 60 mg L<sup>-1</sup>) and different temperatures (30, 40 and 50 °C) varied from 0.06 to 0.82 (Fig. 9b). Thus, the result confirms the feasibility of adsorbent for the removal of Cr<sup>6+</sup>.

*Freundlich isotherm model*

The Freundlich model provides metal sorption as a function of metal concentration at equilibrium in solution without considering other factors such as pH, presence of other metal ions, etc. The saturation stage of metal sorption is not assumed in this model. It assumes that the strongest binding sites are occupied first and the sorption efficiency decreases with increase in number of occupied sites by metal (ions). It can be mathematically expressed as [57]:

$$q = k_f(c_e)^{1/n}. \tag{9}$$

The linearized mathematical form of Freundlich can be expressed as:

$$\log q_e = \log k_f + (1/n) \log c_e, \quad (10)$$

where  $k_f$  is the Freundlich constant related to sorption capacity of adsorbent,  $1/n$  is sorption intensity,  $c_e$  is metal ions concentration at equilibrium and  $q$  is metal concentration adsorbed by the adsorbent. The slope of the graph plotted between  $\log c_e$  and  $\log q_e$  gives a value of  $(1/n)$ , while the intercept gives  $\log k_f$ . In the present study, the maximum adsorption capacity ( $k_f$ ) of the adsorbent was  $2.91 \text{ mg g}^{-1}$  at  $30^\circ \text{C}$  having a  $R^2$  value of 0.726 (Fig. 9c; Table 1).

### Adsorption kinetics

Adsorption is governed by various factors like adsorbent morphology (size, surface area, etc.), porosity, film, pore, and intra-particle diffusion, etc. Adsorption mechanism, kinetic behaviour, and rate constant determination of  $\text{Cr}^{6+}$  on n-ZnO was studied by applying pseudo-first order, pseudo-second order kinetic models, and the intra-particle diffusion model.

#### *Pseudo-first-order kinetic model*

It assumes that the rate of occupation of binding sites is directly proportional to the number of unoccupied sites onto the adsorbing material. The pseudo-first-order rate can be mathematically written as [57]:

$$(dq/dt) = k_1(q_e - q), \quad (11)$$

where  $q_e$  is the metal concentration ( $\text{mg g}^{-1}$ ) adsorbed at equilibrium,  $q$  is the metal concentration adsorbed at time  $t$ ,  $k_1$  is the rate constant of pseudo first order kinetics ( $\text{min}^{-1}$ ). When the above equation is integrated between the limits  $t = 0$  to  $t = t$  and  $q = 0$  to  $q = q_e$ , the equation becomes:

$$\log(q_e - q) = \log q_e - (k_1 \times t)/2.303. \quad (12)$$

A linear plot drawn between  $\log(q_e - q)$  and  $t$  gives the fitness of pseudo first order sorption kinetics.

#### *Pseudo-second-order kinetic model*

It assumes that the rate of occupation of binding sites is directly proportional to the square of the number of unoccupied sites onto the adsorbing material. The pseudo-second-order rate can be mathematically written as [57]:

$$(dq/dt) = k_2(q_e - q)^2, \quad (13)$$

where  $q_e$  is the metal concentration ( $\text{mg g}^{-1}$ ) adsorbed at equilibrium,  $q$  is the metal concentration adsorbed at time  $t$ ,  $k_2$  is a rate constant of pseudo second order kinetics ( $\text{gmg}^{-1}\text{min}^{-1}$ ), which can be determined from the graph plotted between  $t/q$  and  $t$ . When the above equation is integrated between the limits  $t = 0$  to  $t = t$  and  $q = 0$  to  $q = q_e$ , the equation becomes:

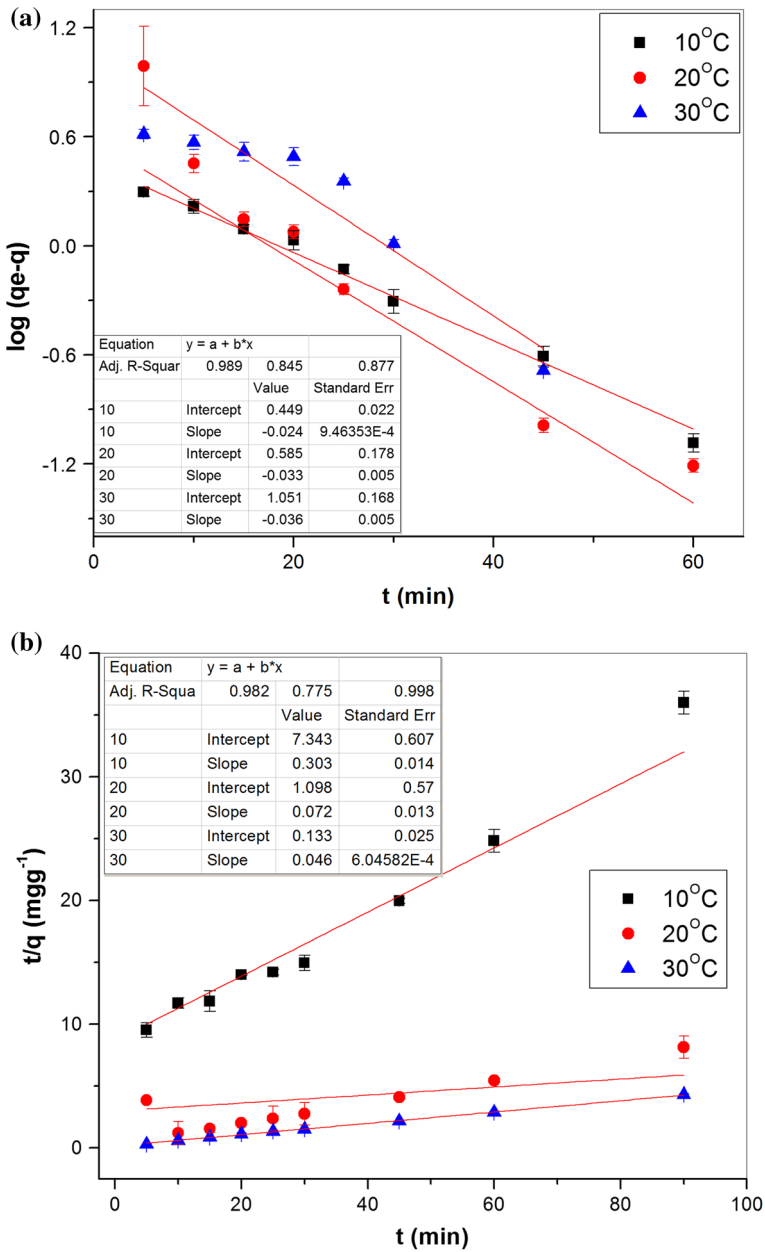


**Fig. 10** a Pseudo first order kinetics. b Pseudo second order kinetics. c Intra-particle diffusion

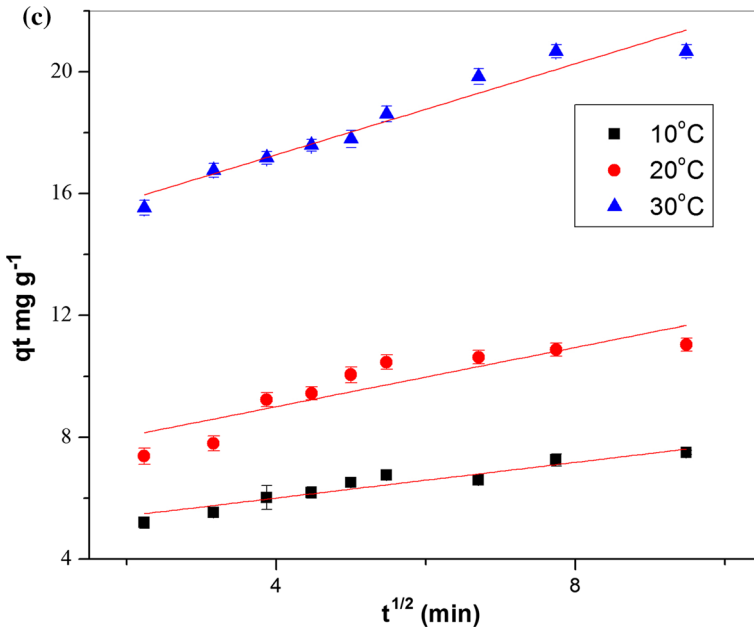


Fig. 10 continued

$$t/q = (1/k_2q_e^2) + (1/q_e)t. \tag{14}$$

The initial rate of adsorption ( $h$ ) ( $\text{mg g}^{-1}\text{min}^{-1}$ ) can be calculated using following equation:

$$h = k_2q_e^2. \tag{15}$$

Pseudo first order and pseudo second order kinetics were applied for the metal ion concentration 10, 20, and 30  $\text{mg L}^{-1}$ . The rate constant of pseudo first order kinetics ( $K_1$ ) for 10, 20, and 30  $\text{mg L}^{-1}$  was  $57.87 \times 10^{-3}$ ,  $89.21 \times 10^{-3}$ , and  $75.14 \times 10^{-3} \text{ min}^{-1}$  having  $R^2$  values 0.990, 0.873, and 0.862, respectively (Fig. 10a). Similarly, the rate constant of pseudo second order kinetics ( $K_2$ ) was  $12 \times 10^{-3}$ ,  $4 \times 10^{-3}$ , and  $15 \times 10^{-3} \text{ g mg}^{-1} \text{ min}^{-1}$  having  $R^2$  values 0.982, 0.775, and 0.998, respectively (Fig. 10b). Comparing  $q_e$  experimental with  $q_e$  model, the pseudo second order kinetics was found more suitable (Table 1).

*Intra-particle diffusion model (Weber–Morris model)*

As the pseudo-first order and pseudo-second order kinetic models are unable to predict the rate limiting steps (i.e., boundary/film layer and intra-particle diffusion), this model helps to assess the contribution of intra-particle diffusion as a rate limiting step (slowest rate during the adsorption). Intra-particle rate constant ( $K_{\text{diff}}$ ) may be determined by the following equation [56, 58, 59]:



$$q_t = K_{\text{diff}}(t^{0.5}) + C, \quad (16)$$

where  $q_t$  is the adsorption capacity at time  $t$ ,  $K_{\text{diff}}$  is the intra-particle diffusion constant ( $\text{mg g}^{-1} \text{min}^{-1/2}$ ), and  $C$  is the thickness of the film. The effect of the boundary layer increases with increase in  $C$ . Slope and intercept of plot ( $q_t$  vs.  $t^{0.5}$ ) gives the value of  $K_{\text{diff}}$  and  $C$ . The diffusion model is divided into two steps; transfer of adsorbate to adsorbent and intra-particle diffusion in adsorbent. For the intra-particle diffusion as rate limiting steps, the plot line should pass through the origin, which it is not passing in the present study (Fig. 10c). Therefore, intra-particle diffusion is not a rate limiting factor in this study.

### Thermodynamics study

The effect of temperature on adsorption capacity can be simulated by applying the thermodynamic model. The feasibility, change in enthalpy ( $\Delta H^\circ$ ), entropy ( $\Delta S^\circ$ ), and free energy ( $\Delta G^\circ$ ) can be easily predicted using the following equations [58]:

$$\Delta G^\circ = -RT \ln K_c, \quad (17)$$

$$\log K_c = (\Delta S^\circ / 2.303R) - (\Delta H^\circ / 2.303RT), \quad (18)$$

$$\Delta G^\circ = \Delta H^\circ - T\Delta S^\circ, \quad (19)$$

where  $K_c$  ( $\text{Lg}^{-1}$ ) is the equilibrium constant,  $T$  is temperature (Kelvin), and  $R$  is the gas constant ( $8.324 \text{ J mol}^{-1} \text{K}^{-1}$ ). Change in enthalpy ( $\Delta H^\circ$ ) and entropy ( $\Delta S^\circ$ ) were calculated from slope and intercept of the Van't Hoff graph plotted between  $\log K_c$  and  $1/T$ . Change in free energy was found to be negative at all the temperatures indicating the spontaneous nature of adsorption (Table 2). However, a positive change in enthalpy denotes the endothermic nature of the reaction, which is supported by the study of change in temperature on adsorption. Similarly, the positive change in entropy ( $\Delta S^\circ$ ) signifies an increase in randomness between adsorbent/adsorbate interfaces during the adsorption [58].

### Application to wastewater

Synthesized adsorbent was applied on secondary treated wastewater collected from the Bhagwanpur sewage treatment plant in Varanasi, India. Wastewater samples were collected in pre-washed and acidified PTFE bottles and transported

**Table 2** Thermodynamic values of different parameters

| Temperature (K) | $K_L$ ( $\text{L mol}^{-1}$ ) | $\Delta G^\circ$ ( $\text{KJ mol}^{-1}$ ) | $\Delta H^\circ$ ( $\text{KJ mol}^{-1}$ ) | $\Delta S^\circ$ ( $\text{KJ mol}^{-1} \text{K}^{-1}$ ) |
|-----------------|-------------------------------|---|---|---|
| 303             | 3450.65                       | -20.50                                    | 61.83                                     | 0.27  |
| 313             | 4146                          | -21.65                                    |   |   |
| 323             | 15,982.41                     | -25.96                                    |   |   |

**Table 3** Comparative study of different adsorbents for Cr<sup>6+</sup> removal

| Adsorbent              | Adsorption capacity (mg g <sup>-1</sup> ) (Adsorbate)                           | References    |
|------------------------|---|---------------|
| n-ZnO                  | 26.7 (30 mg L <sup>-1</sup> ) (Cr <sup>6+</sup> )                               | Present study |
| n-ZnO                  | 59.89 (Zn <sup>2+</sup> ), 94.38 (Cd <sup>2+</sup> ), 133.5 (Hg <sup>2+</sup> ) | [56]          |
| n-ZnO                  | ~ 86 (Cd)   | [44]          |
| Activated carbon       | ATFAC 16.1 (40 °C) (Cr <sup>3+</sup> )<br>ACF 40.29 (40 °C) (Cr <sup>3+</sup> ) | [16]          |
| Spent activated clay   | 1.42 (40 °C) (Cr <sup>6+</sup> )  | [24]          |
| Magnetic iron oxide    | 3.56 (Cr <sup>6+</sup> )<br>11.53 (Ni <sup>2+</sup> )                           | [53]          |
| River bed sand         | 0.15 (Cr <sup>6+</sup> )  | [23]          |
| Modified riverbed sand | 0.79 (Cr <sup>6+</sup> )  | [56]          |
| Fly ash                | 1.4 (Cr <sup>6+</sup> )   | [61]          |
| Raw rice bran          | 0.07 (Cr)   | [62]          |
| Rice husk              | 0.6 (Cr)  | [63]          |
| Saw dust               | 0.893 (Cr)  | [63]          |
| Wollastonite           | 0.83 (Cr <sup>6+</sup> )  | [64]          |
| n-Iron oxide/hydroxide | 11.18 (Cr)  | [66]          |

immediately to the laboratory following standard protocol [60]. After analyzing initial metal ion concentration, the samples were treated with n-ZnO under optimum conditions obtained by the batch experiments conducted above. Removal efficiency was as high as 94.6 %, which was still lower than the results obtained above. This may be due to the interference caused by the presence of other impurities in the wastewater. The toxicity of nano ZnO particles has been discussed elsewhere [67, 68]. Therefore, after the application of nano particles, extra care is required to filter out residual nano adsorbent particles from the treated wastewater. Consequently, the adsorbent (n-ZnO) may be used for removal of Cr<sup>6+</sup> ion from wastewater discharged from anthropogenic sources. The comparative study of the removal efficiency of various adsorbents is given in Table 3.

## Conclusion

The present study dealt with synthesis and application of n-ZnO for the removal of Cr<sup>6+</sup>. Results revealed that n-ZnO is a highly potent metal oxide adsorbent, which may remove up to 100 % chromium hexavalent ions in acidic conditions (pH 2.0) following pseudo-second order kinetics at higher temperature (50 °C). The adsorption process was endothermic and the degree of randomness increased during the process. The Langmuir isotherm model was found most suitable, which was confirmed by a separation factor value ( $0 < R_L < 1$ ) suggesting a homogenous surface with monolayer adsorption having constant adsorption energy. Thus, n-ZnO may be used on a pilot scale for the removal of hexavalent Cr ion from wastewater.

**Acknowledgments** The authors are thankful to University Grants Commission, India for providing financial support (UGC-REF. No. 20591, NET-DEC. 2009) and the Institute of Environment and Sustainable Development and Department of Botany, Banaras Hindu University, Varanasi, India for providing necessary infrastructure. The authors also want to acknowledge the Head, Department of Metallurgy, for SEM analysis which was done at the National Microscopy Centre, Department of Metallurgy, Indian Institute of Technology-Banaras Hindu University. The authors are also thankful to three anonymous reviewers whose valuable suggestions significantly increased the level of the present work. I would like to thank Ashutosh Kumar Pandey and Ashutosh Mishra for their assistance in collecting data and material for the preparation of the manuscript.

## References

1. J. Gómez-Pastora, E. Bringas, I. Ortiz, *Chem. Eng. J.* **256**, 187–204 (2014)
2. M. Chabukdhara, A.K. Nema, *Chemosphere* **87**, 945–953 (2012)
3. A.K. Mishra, B. Mohanty, *Environ. Toxicol. Pharmacol.* **26**, 136–141 (2008)
4. A.S.H. Alhashemi, A.R. Karbassi, B.H. Kiabi, S.M. Monavari, S.M.B. Nabavi, M.S. Sekhvatjou, *Biol. Trace Elem. Res.* **142**, 500–516 (2011)
5. M.F. Abdel-Sabour, *Electron. J. Environ. Agr. Food. Chem.* **6**, 2178–2198 (2007)
6. T. Liu, Z.-L. Wang, X. Yan, B. Zhang, *Chem. Eng. J.* **245**, 34–40 (2014)
7. D. Mohan, C.U. Pittman Jr., *J. Hazard. Mater.* **B137**, 762–811 (2006)
8. K.Z. Setshedi, M. Bhaumik, S. Songwane, M.S. Onyango, A. Maity, *Chem. Eng. J.* **222**, 186–197 (2013)
9. D. Mohan, K.P. Singh, V.K. Singh, *Ind. Eng. Chem. Res.* **44**, 1027–1042 (2005)
10. Bureau of Indian Standards, Indian standard specifications for drinking water IS: 10500, 1993
11. M.A. Behnajady, S. Bimeghdar, *Chem. Eng. J.* **239**, 105–113 (2014)
12. E. Pehlivan, T. Altun, *J. Hazard. Mater.* **155**, 378–384 (2008)
13. S. Qaiser, A. Saleemi, R. Ahmad, M. Mahmood, *Electron. J. Biotechnol.* **10**, 409–416 (2007)
14. A. Agrawal, K.K. Sahu, *J. Hazard. Mater.* **137**, 915–924 (2006)
15. D. Mohan, K.P. Singh, S. Sinha, D. Gosh, *Carbon* **42**, 2409–2421 (2004)
16. D. Mohan, K.P. Singh, V.K. Singh, *J. Hazard. Mater.* **B135**, 280–295 (2006)
17. S. Mohan, G. Sreelakshmi, *J. Hazard. Mater.* **153**, 75–82 (2008)
18. H. Gao, Y.G. Liu, G.M. Zeng, W.H. Xu, T. Li, W.B. Xia, *J. Hazard. Mater.* **150**, 446–452 (2008)
19. K.A. Fayemiwo, O.H. Awojide, G. Tolu, *Int. J. Eng. Sci. Technol.* **5**, 1245–1248 (2013)
20. R. Elangovan, L. Philip, K. Chandraraj, *Chem. Eng. J.* **141**, 99–111 (2008)
21. K. Seki, N. Saito, M. Aoyama, *Wood Sci. Technol.* **31**, 441–447 (1997)
22. Y.C. Sharma, C.H. Weng, *J. Hazard. Mater.* **142**, 449–454 (2007)
23. Y.C. Sharma, B. Singh, A. Agrawal, C.H. Weng, *J. Hazard. Mater.* **151**, 789–793 (2008)
24. C.-H. Weng, Y.C. Sharma, S.-H. Chu, *J. Hazard. Mater.* **155**, 65–75 (2008)
25. Y.C. Sharma, *Colloids Surf. A Physicochem. Eng. Asp.* **215**, 155–162 (2003)
26. D. Kratochvil, B. Volesky, *Trends Biotechnol.* **16**, 291–300 (1998)
27. D. Park, Y.-S. Yun, H.Y. Cho, J.M. Park, *Ind. Eng. Chem. Res.* **43**, 8226–8232 (2004)
28. E.S. Cossich, C.R.G. Tavares, T.M.K. Ravagnani, *Electron. J. Biotechnol.* **5**(2), 133–140 (2002)
29. J.A. Coston, C.C. Fuller, J.A. Davis, *Geochim. Cosmochim. Acta* **59**, 3535–3547 (1995)
30. M.A. El-Sayed, *Accounts. Chem. Res.* **34**, 257–264 (2001)
31. A. Henglein, *Chem. Rev.* **89**, 1861–1873 (1989)
32. M. Hua, S. Zhang, B. Pan, W. Zhang, L. Lv, Q. Zhang, *J. Hazard. Mater.* **211–212**, 317–331 (2012)
33. J.E. Vanbenschoten, B.E. Reed, M.R. Matsumoto, P.J. McGarvey, *Water Environ. Res.* **66**, 168–174 (1994)
34. S. Babel, T.A. Kurniawan, *J. Hazard. Mater.* **97**, 219–243 (2003)
35. P. Bose, M.A. Bose, S. Kumar, *Adv. Environ. Res.* **7**, 179–195 (2002)
36. N. Boujelben, J. Bouzid, Z. Elouear, *J. Hazard. Mater.* **163**, 376–382 (2009)
37. N. Boujelben, J. Bouzid, Z. Elouear, M. Feki, *Environ. Technol.* **31**, 1623–1634 (2010)
38. G.N. Manju, K.A. Krishnan, V.P. Vinod, T.S. Anirudhan, *J. Hazard. Mater.* **91**, 221–238 (2002)
39. B.J. Pan, J. Wu, B.C. Pan, L. Lv, W.M. Zhang, L.L. Xiao, X.S. Wang, X.C. Tao, S.R. Zheng, *Water Res.* **43**, 4421–4429 (2009)
40. R.P. Han, W.H. Zou, H.K. Li, Y.H. Li, J. Shi, *J. Hazard. Mater.* **137**, 934–942 (2006)

41. S.M. Lee, W.G. Kim, J.K. Yang, D. Tiwari, *Environ. Technol.* **31**, 445–453 (2010)
42. S. Utamapanya, K.J. Klabunde, J.R. Schlup, *Chem. Mater.* **3**, 175–181 (1991)
43. K.E. Engates, H.J. Shipley, *Environ. Sci. Pollut. R.* **18**, 386–395 (2011)
44. V. Srivastava, D. Gusain, Y.C. Sharma, *Ceram. Int.* **39**, 9803–9808 (2013)
45. B. Jeong, D.H. Kim, E.J. Park, M.-G. Jeong, K.-D. Kim, H.O. Seo, Y.D. Kim, S. Uhm, *Appl. Surf. Sci.* **307**, 468–474 (2014)
46. A. Kołodziejczak-Radzimska, T. Jesionowski, *Mater* **7**, 2833–2881 (2014)
47. H.B. Zeng, W.P. Cai, P.S. Liu, X.X. Xu, H.J. Zhou, C. Klingshirn, H. Kalt, *ACS Nano* **2**, 1661–1670 (2008)
48. T.P. Chou, Q.F. Zhang, G.E. Fryxell, G.Z. Cao, *Adv. Mater.* **19**, 2588–2592 (2007)
49. Z.H. Jing, J.H. Zhan, *Adv. Mater.* **20**, 4547–4551 (2008)
50. X.B. Wang, W.P. Cai, Y.X. Lin, G.Z. Wang, C.H. Liang, *J. Mater. Chem.* **20**, 8582–8590 (2010)
51. Y-d Wang, C-l Ma, X-d Sun, H-d Li, *Inorg. Chem. Commun.* **5**, 751–755 (2002)
52. A. Moezzi, A.M. McDonagh, M.B. Cortie, *Chem. Eng. J.* **185–186**, 1–22 (2012)
53. Y.C. Sharma, V. Srivastava, *J. Chem. Eng. Data* **56**, 819–825 (2011)
54. S.-W. Bian, I.A. Mudunkotuwa, T. Rupasinghe, V.H. Grassian, *Langmuir* **27**, 6059–6068 (2011)
55. X.G. Zhang, *Corrosion and Electrochemistry of Zinc*, Publisher-Springer Science + Business Media, New York, pp. 119–171. ISBN: 978-1-4757-9879-1
56. S. Yadav, V. Srivastava, S. Banerjee, C.-H. Weng, Y.C. Sharma, *Catena* **100**, 120–127 (2012)
57. S.K. Mehta, J.P. Gaur, *Crit. Rev. Biotechnol.* **25**, 113–152 (2005)
58. T. Sheela, Y.A. Nayaka, R. Viswanatha, S. Basavanna, T.G. Venkatesha, *Powder Technol.* **217**, 163–170 (2012)
59. W.J. Weber, J.C. Morris, *J. Sanit. Eng. Div.* **90**, 79–107 (1964)
60. Standard methods for examination of water and wastewater, APHA, AWWA (2005)
61. S.S. Banarjee, M.V. Joshi, R.V. Jayaram, *Sep. Sci. Technol.* **39**, 1611–1629 (2004)
62. E.A. Oliveira, S.F. Montanher, A.D. Andrade, J.A. Nóbrega, M.C. Rollemberg, *Process Biochem.* **40**(11), 3485–3490 (2005)
63. K.M.S.S. Sumathi, R.M. Naidu, *Bioresour. Technol.* **96**, 309–316 (2005)
64. Y.C. Sharma, *J. Colloid Interf. Sci.* **233**, 265–270 (2001)
65. G.S. Agarwal, H.K. Bhuptawat, S. Chaudhari, *Bioresour. Technol.* **97**, 949–956 (2006)
66. D. Gussain, V. Srivastava, M. Sillanpaa, Y.C. Sharma, *Res. Chem. Intermediat.* (2016). doi:[10.1007/s11164-016-2523-x](https://doi.org/10.1007/s11164-016-2523-x)
67. B.C. Heng, X. Zhao, S. Xiong, K.W. Ng, F.Y.-C. Boey, J.S.-C. Loo, *Food Chem. Toxicol.* **48**(6), 1762–1766 (2010)
68. A. Sirelkhatim, S. Mahmud, A. Seenii, N.H.M. Kaus, L.C. Ann, S.K.M. Bakhori, H. Hasan, D. Mohamad, *Nano-Micro Lett.* **7**(3), 219–242 (2015)
69. Z. Yang, C. Xie, *Colloid Surf. B* **47**(2), 140–145 (2006)
70. E.A. Meulenkaamp, *J Phys Chem B* **102**(40), 7764–7769 (1998)